

# Nanoscale

Accepted Manuscript



This is an *Accepted Manuscript*, which has been through the Royal Society of Chemistry peer review process and has been accepted for publication.

*Accepted Manuscripts* are published online shortly after acceptance, before technical editing, formatting and proof reading. Using this free service, authors can make their results available to the community, in citable form, before we publish the edited article. We will replace this *Accepted Manuscript* with the edited and formatted *Advance Article* as soon as it is available.

You can find more information about *Accepted Manuscripts* in the [Information for Authors](#).

Please note that technical editing may introduce minor changes to the text and/or graphics, which may alter content. The journal's standard [Terms & Conditions](#) and the [Ethical guidelines](#) still apply. In no event shall the Royal Society of Chemistry be held responsible for any errors or omissions in this *Accepted Manuscript* or any consequences arising from the use of any information it contains.

## ARTICLE

## Plasmonic coupling with most of the transition metals: a new family of broad band and near infrared nanoantennas

Cite this: DOI: 10.1039/x0xx00000x

Received,  
Accepted

DOI: 10.1039/x0xx00000x

[www.rsc.org/](http://www.rsc.org/)

Delphine Manchon<sup>a</sup>, Jean Lermé<sup>a</sup>, Taiping Zhang<sup>b</sup>, Alexis Mosset<sup>a</sup>, Cécile Jamois<sup>b</sup>, Christophe Bonnet<sup>a</sup>, Jan-Michael Rye<sup>a</sup>, Ali Belarouci<sup>b</sup>, Michel Broyer<sup>a</sup>, Michel Pellarin<sup>a</sup> and Emmanuel Cottancin<sup>a\*</sup>

In this article, we show for the first time, both theoretically and empirically, that plasmonic coupling can be used to generate Localized Surface Plasmon Resonances (LSPRs) in transition metal dimeric nano-antennas (NAs) over a broad spectral range (from the visible to the near infrared) and that the spectral position of the resonance can be controlled through morphological variation of the NAs (size, shape, interparticle distance). First, accurate calculations using generalized Mie theory on spherical dimers demonstrate that we can take advantage of the plasmonic coupling to enhance LSPRs over a broad spectral range for many transition metals (Pt, Pd, Cr, Ni,...). The LSPR remains broad for low interparticle distances and masks the various hybridized modes within the overall resonance. However, an analysis of the charge distribution on the surface of the nanoparticles reveals these modes and their respective contributions to the observed LSPR. In the case of spherical dimers, the transfer of the oscillator strengths from the “dipolar” mode to higher orders involves a maximum extinction cross-section for intermediate interparticle distances of a few nanometers.

The emergence of the LSPR has been then experimentally illustrated with parallelepipedal NAs (monomers and dimers) made of various transition metals (Pt, Pd and Cr) and elaborated by nanolithography. Absolute extinction cross-sections have been measured with the Spatial Modulation Spectroscopy technique over a broad spectral range (300-900 nm) for individual NAs, the morphology of which has been independently characterized by electron microscopy imaging. A clear enhancement of the LSPR has been revealed for a longitudinal excitation and plasmonic coupling has been clearly evidenced in dimers by an induced redshift and broadening of the LSPR compared to monomers. Furthermore, the LSPR has been shown to be highly sensitive to slight modifications of the interparticle distance. All the experimental results are well in agreement with finite element method (FEM) calculations in which the main geometrical parameters characterizing the NAs have been derived from electron microscopy imaging analysis. The main advantage of dimers as compared to monomers lies in the generation of a well-defined and highly enhanced electromagnetic field (the so-called “hot spots”) within the interparticle gap that can be exploited in photo-catalysis, magneto-plasmonics or nano-sensing.

## 1. Introduction

The specific optical response of metallic nanostructures to light excitation and the strong enhancement of the electromagnetic (EM) field in their vicinity are governed by a large resonance, known as Localized Surface Plasmon Resonance (LSPR)<sup>1, 2</sup>, which is prominent in optical absorption and scattering spectra and which is related to the collective oscillations of conduction electrons. Its characteristics depend intimately not only on the morphology of the metallic system (size, shape, chemical composition), but also on the immediate environment. The case of closely spaced nanoparticles (NPs) is particularly interesting as it involves plasmonic coupling which generates a higher EM field enhancement, especially in the interparticle region (the so-called “hot spots”)<sup>3, 4</sup>. Accordingly, plasmonic coupling has become a key topic over the last ten years in the field of nano-optics, with the underlying idea of tailoring the optical response of nanoantennas (NAs) by controlling their morphology<sup>3</sup>. This is illustrated for instance in the field of molecular fluorescence detection<sup>5, 6</sup>, Raman scattering measurements<sup>7, 8</sup> and biochemical sensing<sup>9-11</sup>. The most commonly investigated NPs are composed of gold or silver because their LSPR appears in the UV-visible range and can even be tuned to the near-infrared in the case of anisotropic NPs<sup>12-15</sup> or closely spaced NPs (coupled dimers)<sup>4, 16-24</sup>. In this last case, the most striking effect in the optical response is the red-shift of the longitudinal dipolar resonance with decreasing interparticle distance. Moreover, the morphology of the facing sides of interacting NPs has also been found to play a crucial role in the optical response for nearly touching objects (strong coupling regime) as seen in silver nanocube dimers for which a splitting of the LSPR has been observed and demonstrated to be correlated to edge rounding of the opposing faces<sup>25</sup>.

However, extending plasmonic properties to other elements such as the transition metals would open up the range of applications in the field of photo-catalysis<sup>26, 27</sup>, nano-sensing<sup>28</sup> or magneto-plasmonics<sup>29, 30</sup>. Until now, the optical response of the transition metals has not been explored to the same extent as gold or silver because their LSPR appears in the UV range at the nanoscale and is strongly damped and broadened due to the marked influence of interband transitions. It can nevertheless be observed in the blue spectral range with sufficiently large nanoparticles (NPs)<sup>31-36</sup> or in the near-infrared with high aspect ratio anisotropic nano-objects<sup>37</sup>. In this work, we take advantage of the plasmonic coupling in NAs to tailor the LSPR over a broad spectral range (from the visible to the near infrared) by playing on the morphology of NAs (interacting parallelepipeds), of

various transition metals fabricated by nanolithography. With the dielectric function of many transition metals being very similar, the properties demonstrated for one metal can confidently be generalized to several others. To test that this is indeed the case, investigations have been performed on three types of metals (Pd, Pt, Cr). The optical response of individual NAs has been examined using the Spatial Modulation Spectroscopy (SMS) technique which avoids the averaging effects of ensemble measurements and which permits absolute extinction cross-section measurements<sup>38</sup>. Moreover, the optical response has been systematically correlated to the morphology of the NAs through electron microscopy imaging analysis<sup>39</sup>. We demonstrate here that plasmonic coupling occurs in NAs made of the transition metals Pt, Pd and Cr. The results are in good agreement with finite element method (FEM) simulations and can be extended to almost all transition metals.

## 2. Theoretical considerations

The electronic structure of transition metals is characterized by the overlap and hybridization of a nearly free electron-like sp-band with a narrower d-band<sup>40</sup>. When browsing the d-band of the periodic table from the lightest elements to the heaviest ones (from column IIIB to column VIIIIB), the width of the d-band increases, reaching a maximum with the Cr group where the d-band is nearly half filled. The width then decreases until reaching the coinage metals (metals from the column IB (Au, Ag, Cu)), where the d-band is completely filled and its top (highest occupied levels) well below the Fermi level. Furthermore while moving down from 3d-band to 5d-band metals for a given column, the width of the d-band increases due to the progressive influence of relativistic effects<sup>41-43</sup>. The optical response of the metal to an electromagnetic excitation is directly related to its electronic band structure. Consequently, the width of the optical absorption band related to interband transitions is expected to increase in the same way as the d-band. For a large part, interband transitions will therefore be responsible for the optical response of transition metals. Indeed, since the Fermi level lies in the same energy range as the partially filled d-bands, intraband excitations in the sp band will be strongly damped by the interband transition decay mechanism over the entire spectral range (from the UV to the near infrared). In this respect, calculations of the intra- and inter-band contributions to the absorption have shown that interband transitions contribute to absorption already at energies below 0.5 eV<sup>40</sup>. This behavior is reflected in

the dielectric function of the metal which cannot be easily decomposed into a free-electron (Drude-like) contribution and an interband contribution.

In small NPs, due to the high values of the plasmon frequencies for these metals<sup>40</sup>, the LSPR is shifted to the UV range compared to coinage metals and critically damped because of its tight coupling to interband transitions. Although the damping occurs throughout the whole spectral range, its efficiency is determined by the joined density of states and the corresponding oscillator strengths of the d-sp transitions that decrease towards the low energy range. Therefore by shifting the

resonance condition to the lower energy end of the spectrum, the LSPR should emerge more clearly. This is for instance the case when an elongated NP is excited by an EM wave with the electric field polarized along the long axis of the NP. In this respect, extinction cross-sections have been calculated for ellipsoids of various aspect ratios (AR) for several transition metals (Cr, Ni, Pd, Pt) and for gold. Calculations have been performed, first for small sizes in the quasi-static approximation (the scattering is in this case negligible as compared to absorption<sup>44</sup>), and then for large sizes with the Finite Element Method (FEM)<sup>45</sup>.

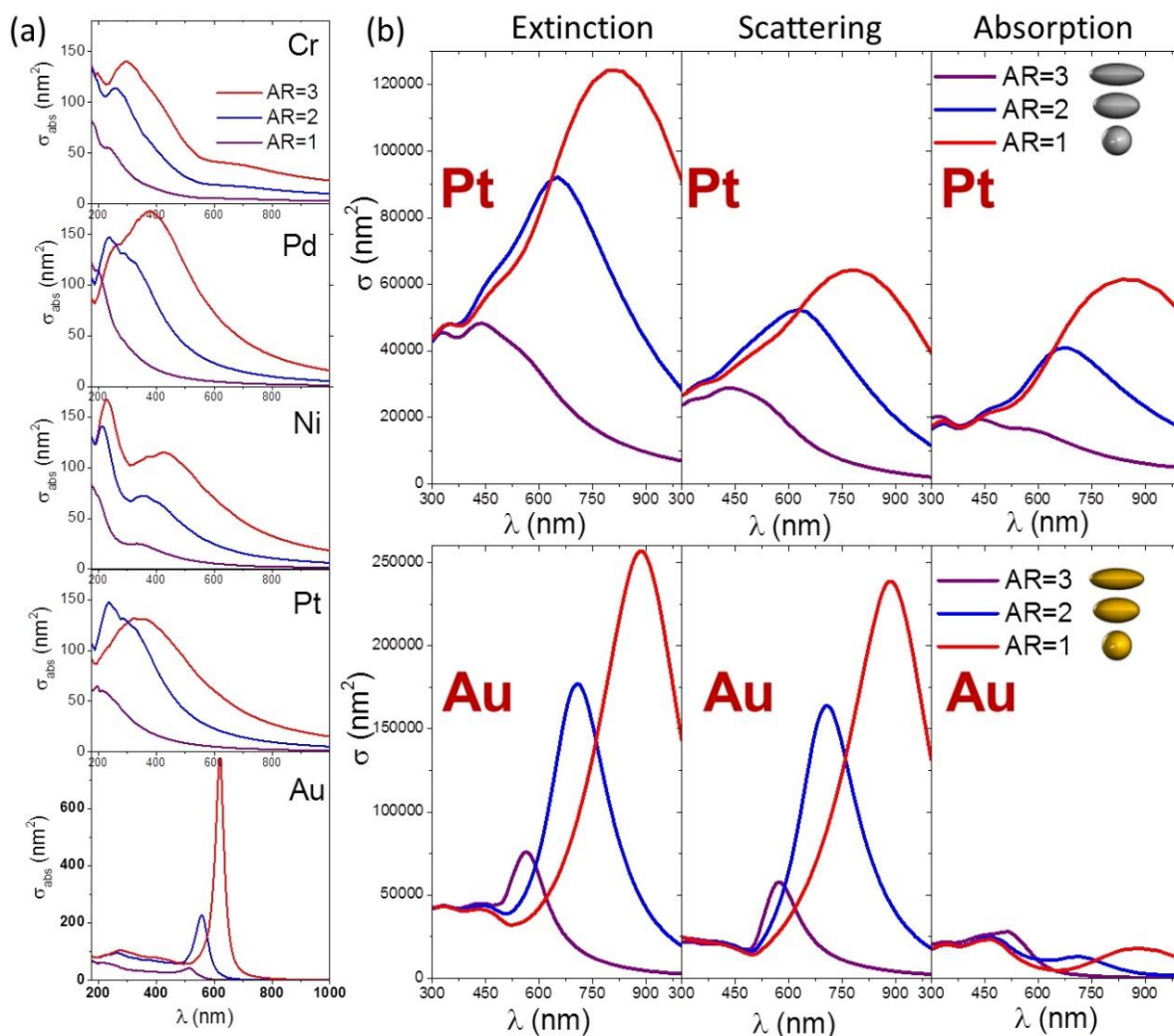


Figure 1: (a) Absorption cross-sections of small spheroidal NPs of Cr, Pd, Ni, Pt and Au for a longitudinal electromagnetic excitation (polarization along the long axis of the spheroid). Mie calculations are performed in the frame of the quasi-static approximation with a constant volume. The spheroids are characterized by their semi-axes  $a$ ,  $b$  and  $c$  and their aspect ratio  $AR=c/a$ . The optical index of the surrounding medium is  $n_{\text{ext}}=1.15$ . (purple)  $a=b=c=5.77$  nm and  $AR=c/a=1$ ; (blue)  $a=b=4.579$  nm,  $c=9,158$  nm,  $AR=2$ ; (red)  $a=b=4$  nm,  $c=12$  nm,  $AR=3$ .

(b) Extinction, scattering and absorption cross-sections of large spheroidal NPs of platinum and gold, calculated with the Finite Element Method (FEM) for a longitudinal electromagnetic excitation. The semi-axes  $a$ ,  $b$  and  $c$  are chosen so as to have a volume corresponding to that of two spheres of 100 nm in diameter. (purple):  $a=b=c=63$  nm and  $AR=c/a=1$ ; (blue):  $a=b=50$  nm,  $c=100$  nm,  $AR=2$ ; (red):  $a=b=43.7$  nm,  $c=131$  nm,  $AR=3$ . The optical index of the surrounding medium is  $n_{\text{ext}}=1.15$  and the optical indices of the metals are extracted from ref.<sup>46,47</sup> for Au, Ni, Cr, Pd, and from ref.<sup>48</sup> for Pt.

In the case of the smallest sizes (Figure 1-a), an LSPR clearly arises in the UV range with increasing aspect ratio for all the considered metals. Compared to gold, the LSPR still remains blue-shifted and is considerably damped and broadened. These differences of behavior originate from differences in their band structure, which is directly reflected in their respective dielectric functions (see Figure S11). In gold, the resonance condition for high aspect ratios is met in an energy range well below the interband transition threshold<sup>1, 44</sup> and thus the damping by the interband transitions is weak. The LSPR thus exhibits a quasi-Drude-Sommerfeld-like behavior with an LSPR of Lorentzian shape. In the case of platinum, plasmonic excitations are always degenerate and strongly coupled with interband transitions. However, the strength of this coupling decreases for NPs of high aspect ratio because the resonance condition is red-shifted. The oscillator strengths correlated to the d-sp transitions of the same order of energy as that of the red-shifted LSPR are therefore weaker and the LSPR can finally emerge. It remains nonetheless spectrally broadened compared to gold.

When the size is increased (Figure 1-b), the extinction cross-section is dominated by scattering for gold NPs and almost evenly distributed between scattering and absorption for platinum NPs. Note that the LSPR intensity in platinum is half that of gold. Similar results are expected for other transition metals as they possess similar dielectric functions (see Figure S11). Compared to the smallest sizes and for a given aspect ratio, the resonance condition is strongly red-shifted. This can be interpreted with Mie theory (for a sphere) by considering the Mie scattering coefficients of the dipole contributions to scattering. A power-series expansion of these coefficients in  $kR$  up to order 3 ( $k$ : wave vector,  $R$ : radius of the sphere) introduces new terms in the expression of the polarizability compared to the quasi-static approximation. These terms result in radiative damping corrections and retardation effects<sup>44</sup> affecting the exciting and dynamic depolarizing fields across the NP diameter<sup>49</sup>. The retarding effects are responsible for the shift of the LSPR as the resonance condition appears for more negative values of the real part of the dielectric function  $\epsilon_1$ . The decrease of  $\epsilon_1$  toward the red spectral range (see Figure S11) results in a strong red-shift of the dipolar plasmon resonance. On the other hand, radiative losses by the oscillating dipole are responsible for a damping and broadening of the LSPR (radiative damping). The same reasoning applies in the case of NPs of high aspect ratios, but the resonance condition is even more red-shifted because of the geometric dependence on the depolarization factors of the

scattering coefficients<sup>44</sup>. In the case of gold, as scattering becomes dominant, the width of the LSPR is no longer due to the Drude-Sommerfeld-like behavior, but rather due, for the most part, to radiative damping. As absorption and scattering reach their maximum at the same wavelength, the overall extinction LSPR is of similar width as the scattering resonance. Notice also that quadrupolar modes begin to emerge in absorption spectra at this point. In the case of transition metals such as platinum, both scattering and absorption are of the same order of magnitude (see Figure 1-b). Both interband transitions and radiative damping contribute to the width of the resonance. Here, however, the resonance maxima of the same order of magnitude appear at different wavelengths for absorption and scattering, and the resulting extinction resonance is slightly broadened as compared to separate scattering and absorption resonances. The relatively large LSPR also conceals the weakly contributing multipolar modes. Another way to ensure the emergence of the LSPR is to employ plasmonic coupling in closely spaced NPs. This provides a new parameter (the interparticle distance) to shape the LSPR and moreover such systems induce a strong enhancement of the EM field in the interparticle region. As an illustration, the optical extinction of a pair of closely spaced spherical NPs has been calculated for different transition metals. Calculations have been performed with the authors' own code using a multiple scattering approach based on the generalized Mie theory<sup>50-53</sup> for NP diameters of 100 nm and for various interparticle distances  $d$ . For a transverse excitation (EM field polarization perpendicular to the dimer axis) the optical response does not reveal a clear resonance and is almost insensitive to the interparticle distance (see dashed lines in Figure 2): the extinction is just twice that of a single sphere. By contrast, for a longitudinal excitation (EM field polarization parallel to the dimer axis), a large LSPR clearly emerges in the visible range for all the investigated metals (Pt, Pd, Cr and Ni). The spectra are qualitatively independent of the metal and the minor differences can be attributed to the small discrepancies in their band structure (see Figure S11). It should be noted that, for all studied metals, there is an optimum of the interparticle distance  $d_{opt}$  around 2-5 nm for which the resonance is more pronounced and slightly narrower. For  $d$  larger than  $d_{opt}$ , the LSPR is still in the blue range and also of weak amplitude because the coupling is weak. For  $d$  lower than  $d_{opt}$ , the LSPR broadens, red-shifts and progressively decreases in amplitude. This optimum is not observed in dimers of gold or silver. Indeed, in this case, the dipolar resonance is red-shifted for decreasing interparticle distances,

steadily amplified<sup>4, 52</sup> and multipolar modes progressively appear.

## ARTICLE

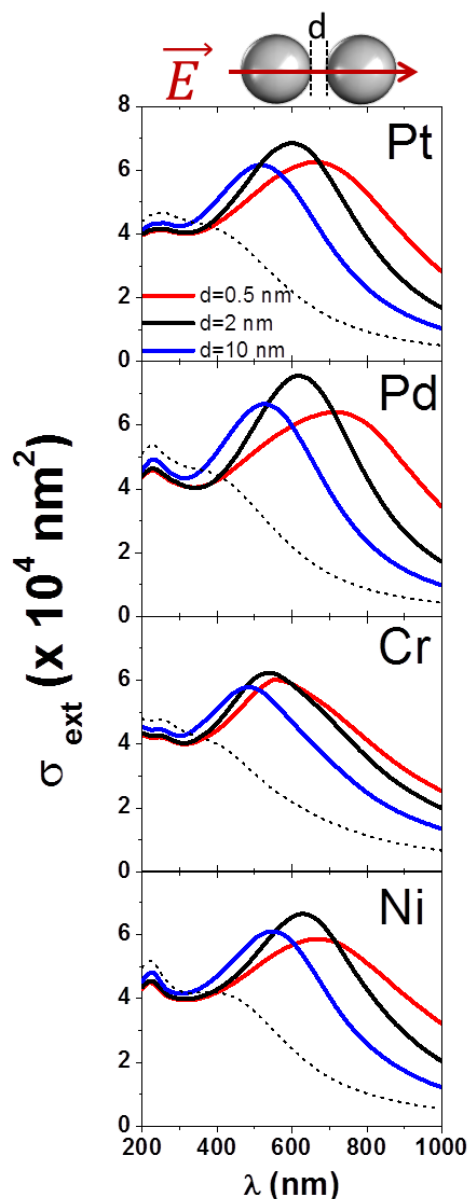


Figure 2: Theoretical extinction cross-sections calculated in the frame of the generalized Mie theory for homometallic dimers of 100 nm  $\varnothing$  spheres made of different transition metals (Pt, Pd, Cr and Ni) with various interparticle distances ( $d=10$  nm (blue),  $d=2$  nm (black),  $d=0.5$  nm (red)). The incident electromagnetic field is polarized along the dimer axis, except for the dashed line curves which correspond to optical extinction cross-sections for a transverse excitation and  $d=2$  nm (for  $d=0.5$  nm and  $d=10$  nm (not shown) the transverse response is nearly indistinguishable from that of  $d=2$  nm). The optical index of the surrounding medium is  $n_{\text{ext}}=1.15$ .

To better understand these distinct behaviors, extinction, scattering and absorption cross-sections of platinum and gold dimers of 100 nm  $\varnothing$  spheres for various interparticle distances

( $d=10, 2$  and  $0.5$  nm)) are compared in Figure 3. The evolution of the spectra with decreasing interparticle distance can be understood, at least qualitatively, through the concept of plasmon hybridization<sup>54</sup>. Indeed the strong mutual interaction is responsible for a coupling between modes of different orders. As the interparticle distance decreases increased coupling leads to the emergence of higher order resonances. This is correlated to the greater influence of the complex near field (superimposed on the incident field) of each NP of the dimer on the other. The most spectacular effect is the redshift of the dipolar resonance (which is actually a hybridized mode) with decreasing interparticle distance<sup>52</sup>. In gold where the resonances arise below the interband transition threshold, the widths are mainly correlated to radiative damping and remain relatively narrow (i.e. absorption remains weak). The multipolar modes are therefore well defined and clearly distinguishable. The more intense red-shifted mode retains a “dipolar” character around the peak as can be seen from the pictures of the charge distributions at the NP surface (Figure 3) for both wavelengths  $\lambda_a$  and  $\lambda_b$  surrounding the “dipolar” peak. One should also notice that the charge distribution is reversed on opposite sides of the resonance maximum. At the wavelength  $\lambda_c$  for which a weaker resonance appears, charges of the same sign are distributed on both extremities of each NP with a ring of opposite charge between them. This charge distribution is the signature of the quadrupolar mode contribution to this hybridized mode<sup>55</sup>. Notice also that the “dipolar” resonance is visibly narrower for smaller interparticle distances (even if strictly speaking one should draw the spectra as a function of energy for a real comparison), because the resonance condition is met below the interband transition threshold. For platinum, the LSPR is far broader because of the strong influence of interband transitions and radiative damping (absorption and scattering are of the same order of magnitude). As in gold, the red-shift with decreasing interparticle distances is manifest, and the transfer of the oscillator strengths to the modes of higher orders is expected to occur, but such modes are masked by this very broad resonance. Nonetheless, looking at the charge distribution on the NP surfaces for various wavelengths indicate that the broad resonance is the convolution of several modes. For instance, close to the maximum absorption peak (for wavelength  $\lambda_1$ ), the charge distribution is typical of a “dipolar” mode. By slightly shifting to the maximum of the scattering peak ( $\lambda_2$ ), the charge distribution becomes more characteristic of a hybridized mode involving quadrupolar modes. This mode becomes prominent as the energy increases (see the charge distribution at  $\lambda_3$ ). This shows that the mechanism of oscillator strength transfer from the dipolar mode to modes of higher orders with decreasing

interparticle distance is very general and holds for gold, platinum and any other transition metals. The main difference between transition and coinage metals is the large intrinsic broadening of the corresponding resonance that prevents their spectral identification since they are convoluted in a single and wide band. This convolution is at the origin of the apparently non-monotonous evolution (red-shift, increasing and narrowing) of the extinction cross-section for platinum when the interparticle distance  $d$  decreases. The optimum distance  $d_{opt}$  for which the extinction cross-section is most clearly defined can be understood as follows. If  $d$  is large, the dipolar

peak dominates but it is strongly broadened because it is only weakly red-shifted. On the contrary, if  $d$  is small, it should be narrower, but it has to be convoluted with the quadrupolar mode that has expanded in the high energy range and that has assumed some of its oscillator strength. This result here is also a large damped overall resonance as in the case of large  $d$ . Both processes explain the occurrence of particular distances ( $d_{opt}$ ) for which band broadening reaches a minimum. The same trends expected for other transition metals (Cr, Pd, Ni, ...) (see Figure 2) should be interpreted in the same way.

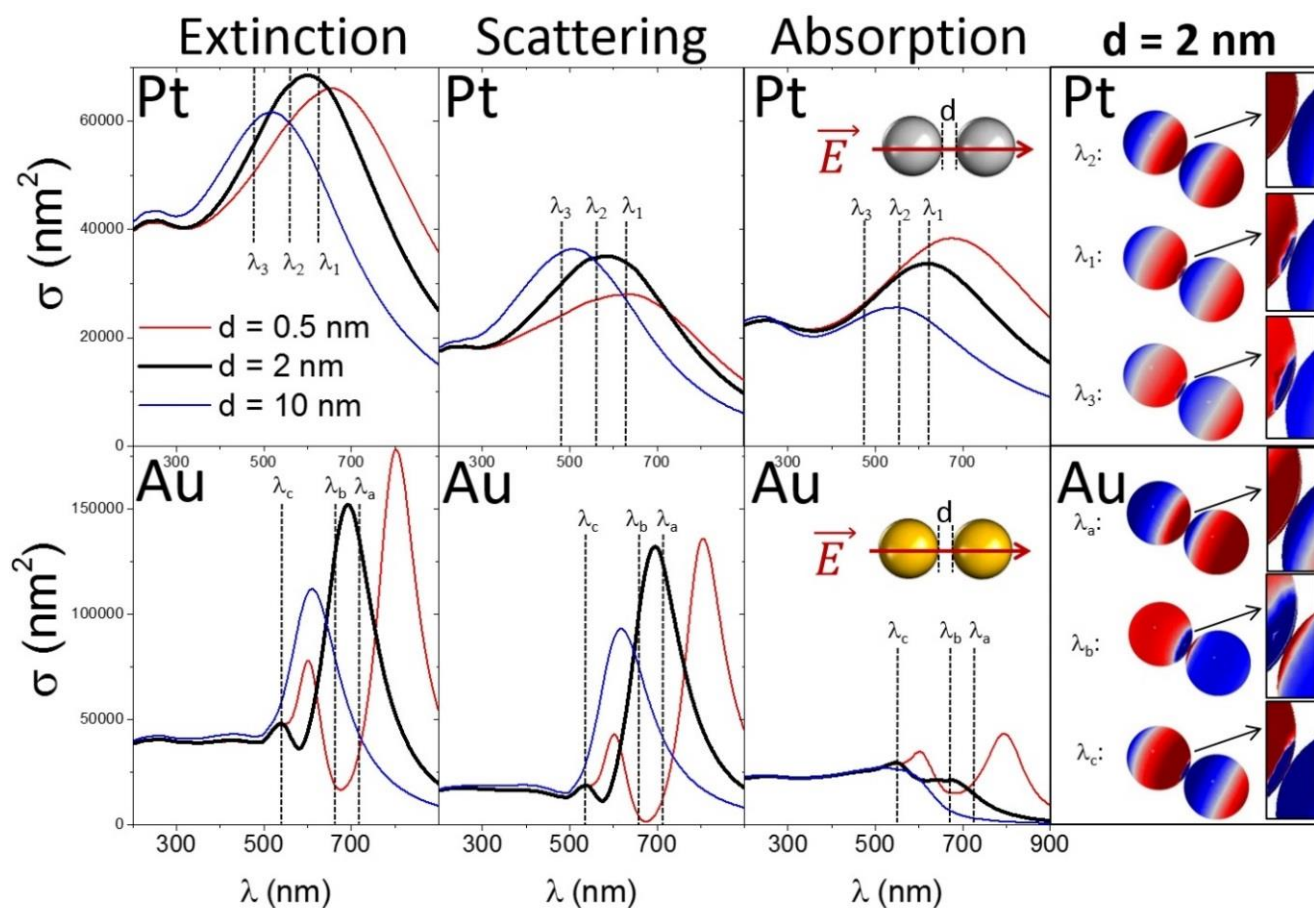


Figure 3: Theoretical extinction, scattering and absorption cross-sections calculated in the frame of the generalized Mie theory for dimers of 100 nm  $\varnothing$  spheres made of platinum (upper row) or gold (lower row) with various interparticle distances  $d$  ( $d=10$  nm (blue),  $d=2$  nm (black),  $d=0.5$  nm (red)) and for an incident electromagnetic field polarized along the dimer axis. The optical index of the surrounding medium is  $n_{ext} = 1.15$ . The charge distribution on the surface of the NPs (for an interparticle distance of  $d=2$  nm) is shown on the right for three selected wavelengths ( $\lambda_1, \lambda_2, \lambda_3$  for platinum and  $\lambda_a, \lambda_b, \lambda_c$  for gold) reported on the spectra. The red and blue colors correspond to opposite charges on the surface of the NPs.

### 3. Materials and methods

#### 2.1 Nanoantenna elaboration and characterization

In order to demonstrate the emergence of an LSPR in anisotropic nano-objects such as single parallelepipeds and, more importantly, in dimers (coupled parallelepipeds), NAs of various transition metals (Cr, Pd and Pt) have been elaborated by nanolithography, the process of which can be summarized as follows. First, a PMMA/MMA double layer of electron-beam

(e-beam) sensitive resist is deposited on a transparent glass substrate by spin-coating. The design pattern is then defined via e-beam lithography using a modified scanning electron microscope (Inspect F-50 FEI). The target interparticle distance could be further tuned with the dose of exposure. Following the development of the positive tone bilayer, a 5 nm layer of chromium is first deposited on the glass, which is then covered by 70 nm of the metal to be studied (Pt, Pd or Cr). The Cr film is used as an adhesive layer between the metal and the substrate in the case of Pt and Pd. The metal is deposited onto the

substrate in a Leybold beam heating evaporator under high vacuum ( $\sim 2.10^{-7}$  Torr) with a deposition rate of  $0.5 \text{ \AA/s}$ . The final step is a lift-off, i.e. a chemical dissolution of the resist layer and of the metal deposited on its surface, leaving only the metal NAs on the glass substrate.

Optical measurements have been performed with a high sensitivity spectrophotometer that relies on the SMS technique<sup>38</sup>. This allows the detection of the overall extinction of light by a single nano-object over a broad spectral range (from the near UV to the near infrared). It consists of irradiating a supported particle by the light beam provided by a Quartz Tungsten Halogen lamp and focused at the diffraction limit by a high numerical aperture reflecting objective. The transmitted light is collected with a second objective, identical to the first one, and sent to a spectrophotometer before being detected by a photomultiplier tube (PMT). A sinusoidal displacement (frequency  $f$ ) is applied to one axis of a high resolution XY piezoelectric stage so that a given particle periodically moves in and out of the light beam. The subsequent modulation of the transmitted light is detected by a lock-in amplifier at frequency  $f$  or  $2f$  which greatly improves the signal-to-noise ratio. An accurate characterization of the spot profile in the sample plane enables the determination of the absolute extinction cross-section  $\sigma_{\text{ext}}$  of a single nano-object from the ratio of the lock-in signal to the average transmitted light signal.

NAs elaborated by nanolithography are separated by a distance of  $4 \text{ }\mu\text{m}$  so that individual NAs can be optically studied. SEM imaging of these objects is carried out after their optical characterization (using a SEM FEI Quanta 250 FEG operating in low vacuum) in order to avoid substrate contamination induced by electron beam impact. We can thus measure the absolute extinction cross-section of a single nano-object from  $300 \text{ nm}$  to  $900 \text{ nm}$  and correlate it to the object's real morphology thanks to electron microscopy imaging<sup>39</sup>. Moreover, an extension of the detection up to  $1600 \text{ nm}$  has been implemented during the course of this study and a few spectra have been performed over the range  $300\text{-}1600 \text{ nm}$ . Note also that 16 NAs of a identical design are elaborated at a time and their design reproducibility has been checked through both SEM and optical measurements.

The parallelepipeds, defined by the pattern design software, are characterized by their target length  $L$  varying between  $50 \text{ nm}$  and  $150 \text{ nm}$ , their width  $w$  ( $50 \text{ nm}$ ) and their height  $h$  ( $70 \text{ nm}$ ). Dimers are furthermore characterized by the target interparticle distance  $d_{\text{target}}$  varying from zero to  $50 \text{ nm}$ . SEM characterizations show that two categories of nano-objects are actually obtained: either touching parallelepipeds or non-touching parallelepipeds with an interparticle distance larger than  $25 \text{ nm}$ . Indeed, for theoretical distances  $d_{\text{target}} < 30 \text{ nm}$ , the parallelepipeds are systematically in contact, whereas they do not touch for  $d_{\text{target}} > 40 \text{ nm}$  where the observed interparticle distance is always greater than  $25 \text{ nm}$  (between  $30$  and  $40 \text{ nm}$ ). One can notice that these results hold for all investigated materials: Pt, Pd and Cr (see Figure SI2).

Figure 4 shows the optical extinction spectra of a monomer and a dimer of platinum parallelepipeds of  $100 \text{ nm}$  length for both

longitudinal and transverse EM excitations. The corresponding SEM and AFM images of the NAs are given on the right side of the figure. The polarization of the exciting EM field is indicated on the SEM image with matching colors between arrows and optical spectra. In both cases no clear LSPR appears for transverse excitations whereas it arises in the visible range for longitudinal excitations. For the monomer, the LSPR is due to the anisotropic shape of the NA. For the dimer, even if the interparticle distance is large, a coupling effect is already obvious as the position of the LSPR is red-shifted and broadened compared to the response of the monomer.

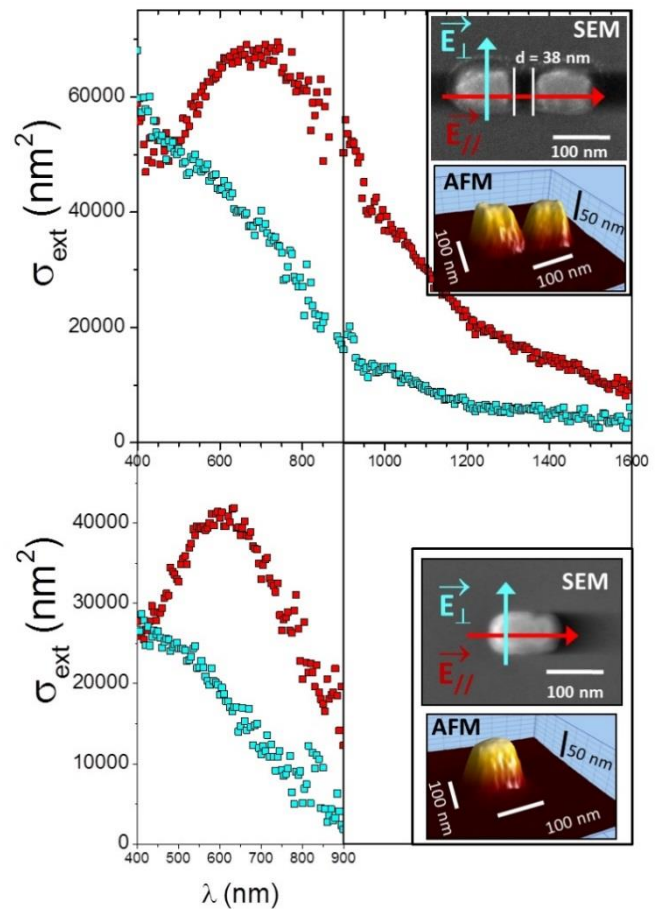


Figure 4: Experimental absolute extinction cross-sections of individual platinum NAs (monomers and dimers) for a longitudinal EM excitation (red) and transverse EM excitation (cyan). The optically investigated NAs have been characterized by Scanning Electron Microscopy (SEM) and Atomic Force Microscopy (AFM) the images of which are shown on the right. The heights deduced by AFM measurements are circa  $70 \text{ nm}$ . The arrows on the SEM images indicate the direction of polarization of the exciting EM field. For the dimer, the extinction cross-section has been measured from  $400 \text{ nm}$  to  $1600 \text{ nm}$ .

### 3.2 Calculations

Extinction cross-sections are calculated using the Finite Element Method (FEM)<sup>45</sup>. Parallelepipeds are defined by their length  $L$ , width  $w$  and height  $h$ . Edges and corners of the perfect parallelepipeds are rounded by replacing edges and corners by quarter-cylinders and spheres of radius  $r_c$ <sup>25</sup>. Given that the NAs are elaborated by nanolithography on a surface, the rounding at

their base is removed (See Figure SI3). Calculations can be performed for NAs deposited on glass substrate of optical index  $n_{\text{sub}}=1.5$  or in a homogeneous medium of optical index  $n_{\text{ext}}$ . Figure SI4 shows the comparison between both calculations for a platinum monomer. For a homogeneous environment,  $n_{\text{ext}}$  remains a free parameter in calculations, and  $n_{\text{ext}}=1.25$  is the optimized value to obtain a good agreement with experimental extinction spectra. The calculated spectrum obtained in the case of the monomer over the semi-infinite glass substrate is found to be damped and blue-shifted compared to experiments. A better agreement is obtained if a local environment of optical index  $n_{\text{env}}=1.15$  surrounding the NA is added so as to mimic the possible presence of impurities adsorbed on the NA surface (see Figure SI4). The LSPR in this case is at the same spectral position as the one obtained for a homogeneous medium of index  $n_{\text{ext}}=1.25$ , but slightly damped. Therefore, and for convenience, all of the following calculations have been performed for NAs in a homogeneous medium of optical index  $n_{\text{ext}}=1.25$ . Based on SEM and AFM imaging the width and height of the NAs were set to  $w=60$  nm and  $h=70$  nm, respectively. The rounding parameter was arbitrarily set to  $r_c=8$  nm. This parameter that has been tested and shown to be of relatively minor importance compared to the dependence on the LSPR of other parameters such as the aspect ratio and the interparticle distance (see Figures SI5 and SI6). The influence of the chromium adhesion layer has also been tested (see Figure SI7), and the optical response with this layer is akin to the one without (a slight damping is barely visible). The chromium layer is therefore ignored in the calculations and the height  $h$  of the NAs used in the calculations is taken to consist of a single metal (Pt, Pd or Cr).

#### 4. Results and discussion

As a first step, the individual parallelepipeds of the three elements (Pt, Pd and Cr) constituting the NAs have been investigated. The optical extinction cross-sections of monomers of various lengths (and thus various aspect ratios) are reported in Figure 5 for an excitation polarization along the long axis of the monomers. For the three metals a large LSPR clearly

emerges in the visible spectral range along with a resonance red-shift and broadening for increasing aspect ratios. The amplitudes of the resonances are similar for Pd and Pt and systematically larger than for Cr (for same size and aspect ratio). Concerning their spectral position, they are less red-shifted for Cr than for Pd and Pt. For example, for monomers of aspect ratio close to 2.5, the LSPR occurs about 550 nm for the chromium monomer (of length  $L=120-125$  nm) while it occurs near 650 nm for Pd and Pt. The evolution of the maximum of the LSPR peak  $\lambda_{\text{RPS}}$  versus the aspect ratio is reported on the right side of the experimental spectra. It evolves almost linearly, the slope being the same for Pd and Pt, and slightly smaller for Cr. The SEM images of the optically investigated monomers, displayed on the top of Figure 5, reveal the geometry of the NAs (length, width and thus aspect ratio) which can then be implemented in FEM simulations. The bottom of Figure 5 shows that FEM simulations agree well with experiments. First, the absolute cross-sections are of the same order of magnitude as the experimental ones for all three metals. Second, the shape and position of the LSPR peaks and their evolution with the aspect ratio are in very good agreement with their experimental counterparts. One can also notice that the experimental LSPR peaks of the chromium NAs are narrower and more symmetric than those expected theoretically. This is probably linked to a better quality of the deposited metal during the nanolithography process performed under high vacuum, compared to the metal films from which optical indices have been deduced<sup>47</sup> and which display irregularities in the visible range (see Figure SI1). Similar arguments as those given for large ellipsoids can be given in the discussion concerning the widths of the resonances that are correlated to both damping by the interband transitions and radiative damping.

## ARTICLE

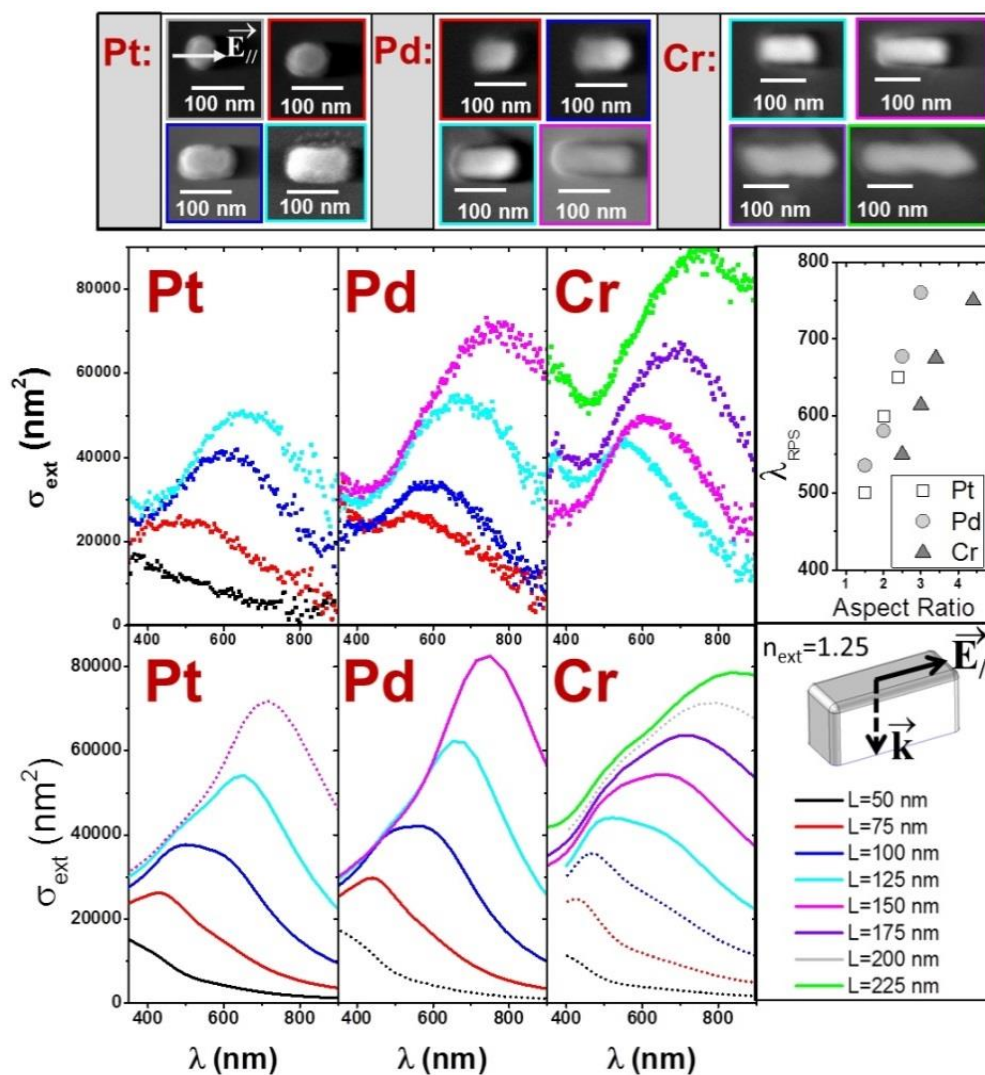


Figure 5: Experimental (top) and theoretical (bottom) absolute extinction cross-sections of individual platinum, palladium and chromium parallelepipedal monomers of various lengths (for a longitudinal EM excitation). The corresponding SEM images of the optically investigated monomers are displayed on the top of the figure (the same colors are used throughout the figure for each object). The direction of the EM field is indicated in the first SEM image on the top left. On the right side is shown the evolution of the experimental LSPR peak maximum  $\lambda_{\text{RPS}}$  as a function of the aspect ratio (defined as the ratio between the length and the width of the parallelepiped). The dimensions of the monomers used in simulations are  $w=60$  nm,  $r_c=8$  nm and  $h=70$  nm.  $L$  varies from 50 nm to 225 nm (see legend at the right bottom, valid for experimental and theoretical spectra). In calculations the NAs are assumed to be embedded in a homogeneous medium of optical index  $n_{\text{ext}}=1.25$ .

Figure 6 shows a comparison of the optical extinction cross-sections measured for dimers and monomers of identical geometries ( $L=125$  nm, 100 nm and 150 nm for Pt, Pd and Cr, respectively). The LSPR appears systematically red-shifted and broadened for dimers compared to monomers for all the investigated metals. The redshift and broadening are important for relatively large interparticle distance, showing that the coupling effect is already effective. Parallelepipeds of smaller aspect ratio have also been investigated and the coupling effect

is likewise clearly observed (see for example the platinum dimer ( $L=75$  nm,  $d=30$  nm) in Supporting Information (Figure SI8)). These features (LSPR intensity, shift and broadening) are well reproduced for all three elements in FEM simulations. For chromium, as well as in monomers, the experimental LSPRs are narrower than those calculated.

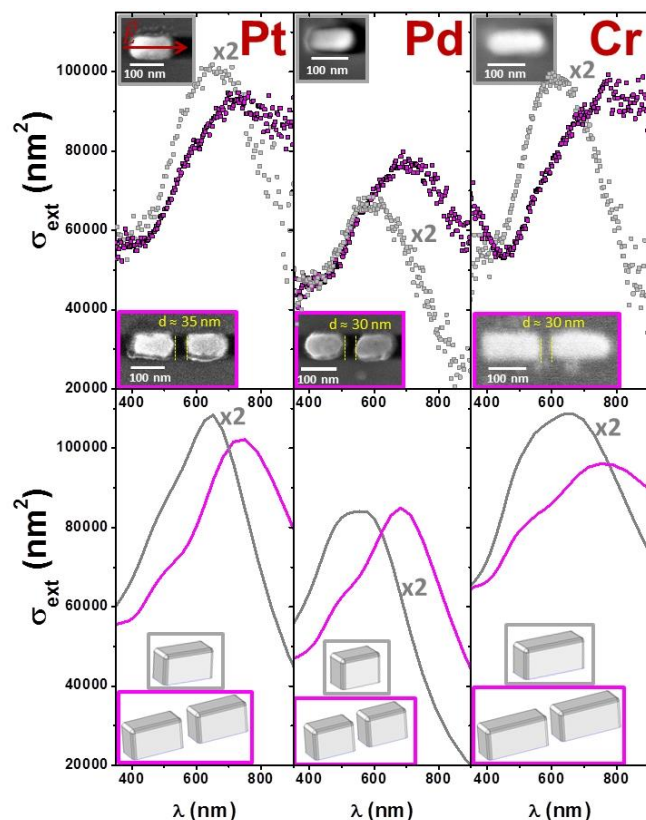


Figure 6: Comparison between monomer and dimer extinction cross-sections for Pt, Pd and Cr (upper row: empirical data, lower row: FEM calculations) for a longitudinal excitation. The monomer extinction cross-sections (gray squares or lines) are multiplied by 2 for qualitative comparison with the dimer extinction cross-sections (magenta squares or lines). The morphology of the NAs has been determined by SEM analysis and used in the calculations. In the calculations the NAs are assumed to be embedded in a homogeneous medium of optical index  $n_{\text{ext}}=1.25$ .

For Pt and Pd it was also possible to slightly vary the interparticle distance between both parallelepipeds. The differences in the corresponding optical extinction spectra are shown in Figure 7. A red-shift of the LSPR is observed, even for a weak decrease of the interparticle distance (from 38 to 31 nm), which shows the high sensitivity of the LSPR to the interparticle gap. These optical spectra are also compared to the ones of touching dimers and total length equal to the sum of parallelepiped lengths and the interparticle distance (NAs obtained for target interparticle distance lower than 30 nm (see Figure SI2)). The NAs have in this case a peanut-like shape and their resonances are shifted to the near infrared region and considerably broadened (the maximum of the LSPR peak is not experimentally accessible). It corresponds to the optical extinction expected for NAs of very high aspect ratios as they form a single nano-object<sup>4</sup>. All these tendencies are well reproduced by simulations using the parameters  $L$  and  $d$  deduced from SEM observations (bottom of Figure 7). By varying the interparticle distance, the shift and enhancement of the LSPR remain small but in good agreement with experiments. The LSPR intensities are however overestimated in the case of Pd. This can be explained by differences in the

total amount of metal as the geometries may differ between experiments and modelling. Indeed the AFM observations (Figure 4) show trapezoidal geometries and a parallelepipedal shape was chosen in calculations. Such a difference does not induce significant changes in the LSPR shape and spectral position, but the amount of metal will be larger in the model, thus leading to a larger LSPR intensity. Concerning the peanut-like NAs, they have been modelled by inserting a parallelepipedal bridge (of height  $h$  and width  $w=35$  nm deduced from SEM observations) between both parallelepipeds. The tendency of the LSPR to move towards larger wavelengths seems to be well reproduced, even if only a part of the spectrum was experimentally accessible.

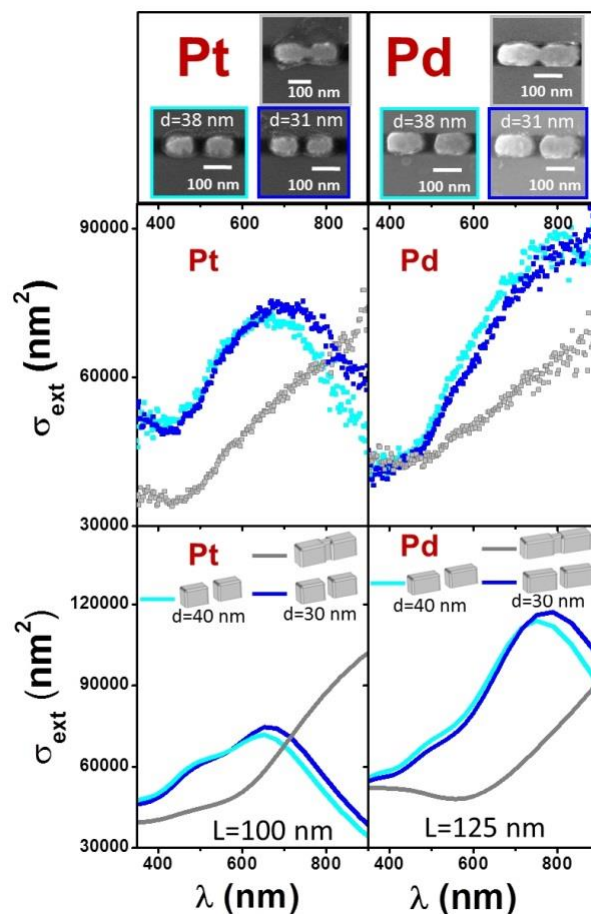


Figure 7: Experimental and theoretical optical extinction cross-sections and corresponding SEM images of Pt and Pd dimers for two different interparticle distances and for two touching parallelepipeds of total length equal to that of the non-touching dimers with the interparticle distance included. In calculations the NAs are assumed to be embedded in a homogeneous medium of optical index  $n_{\text{ext}}=1.25$ .

Unfortunately, the interparticle distance could not be reduced to values lower than 25-30 nm due to limitations of the fabrication process. In the near future we will attempt to reduce it to a few nanometers by using Focused Ion Beam (FIB) to “bisect” monomers of high aspect ratio<sup>56</sup>. This should make it possible to obtain higher enhancement and redshift of the LSPR as predicted by simulations. With this in mind, Figure 8 displays

the predicted evolution of the LSPR with decreasing interparticle distance between monomers of length  $L=100$  nm. From  $d=30$  nm to  $d=1$  nm, a clear enhancement of the LSPR peak is expected while the induced redshift is found around 200 nm. By way of comparison the expected extinction cross-sections of gold dimers is also reported in Figure 8. As in the case of spherical dimers, one can observe that the enhancement for platinum is only 2-3 times smaller than for gold, suggesting that transition metals remain good candidates for plasmonic applications. Another difference is the larger width of the resonance in transition metal based NAs (due to the prevalence of the damping by interband transitions), which can clearly be an advantage for special applications. As in the case of dimers, a view of the charge distribution at the surface of the parallelepipeds for different wavelengths show that the hybridized modes evolve from a “dipolar” character to a “quadrupolar” character by scanning the wavelength from large to small values through the broad LSPR band (see Figure S19). One must also keep in mind that in gold NAs, extinction consists mostly of scattering whereas scattering and absorption are still of the same order in transition-metal-based NAs for the sizes considered here. This difference may also be crucial for non-linear optics<sup>27</sup>.

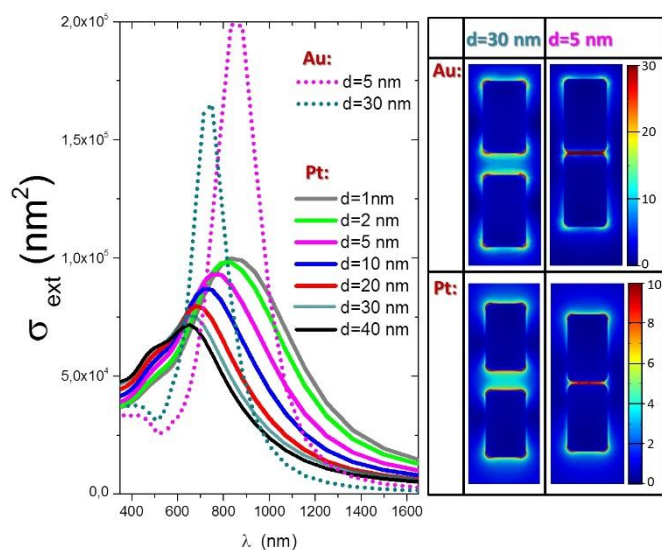
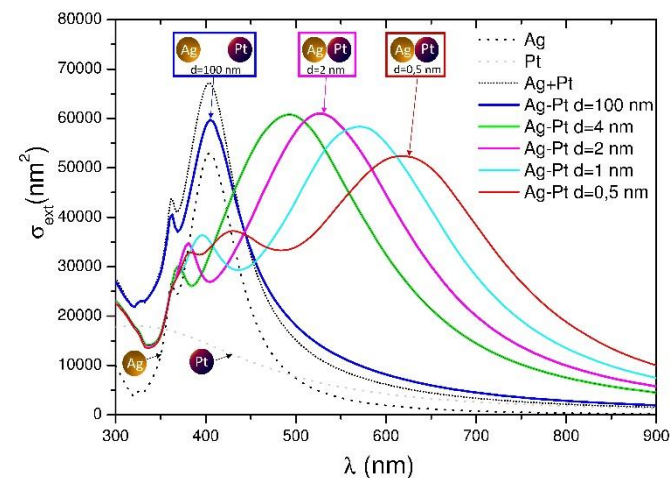


Figure 8: (left) Calculated extinction cross-sections of platinum and gold parallelepipedal dimers ( $L=100$  nm,  $w=60$  nm,  $h=70$  nm) for several interparticle distances. (right) Cross-section views of the EM field magnitude (for the wavelength corresponding to the LSPR maximum) in the plane corresponding to the bottom of the NAs for two interparticle distances ( $d=5$  nm and  $d=30$  nm). The NAs are assumed embedded in a homogeneous medium of optical index  $n_{\text{ext}}=1.25$ .

Finally it should be underlined that the use of dimers instead of monomers is particularly interesting in two ways. First, two parameters can be optimized to tailor the LSPR: the aspect ratio of each monomer and the interparticle distance. It should also be possible to control the shape of the LSPR through careful design of the NAs. For instance, bowtie geometries should lead to narrower LSPRs. However, the main advantage of the dimer geometry probably lies in providing a well-defined region

where the near EM field is considerably enhanced. This is shown in the EM field distribution (plane at the bottom of the NAs) on the right of Figure 8. The enhancement increases with decreasing interparticle distance. The enhancement factor for platinum is only 3 times smaller than for gold (the intensity will then be almost ten times smaller). This region of the enhanced EM field acts as a “hot spot” that can be exploited for photocatalysis or single molecule detection<sup>57</sup>.

The broad LSPR in transition-metal-based systems can be coupled to a narrower LSPR such as the one expected for silver. This should induce interactions between broad and narrow resonances in order to give birth to Fano resonances<sup>58-60</sup>. In that respect, we have calculated the optical response of platinum-silver hetero-dimers in the frame of the generalized Mie theory. Figure 9 shows the expected extinction cross-section for NP diameters of 80 nm and for various interparticle distances  $d$ . In this very particular case, small variations of the interparticle distance induce oscillation shifts in the optical extinction cross-section due to the coupling and interference between the narrow silver with the large platinum (quasi-continuum) LSPRs. This profile is analogous to the typical Fano resonance and its high sensitivity to the interparticle distance illustrates the great potential of transition-metal-based NAs in the field of



plasmonic coupling and sensing.

Figure 9: theoretical optical extinction cross-sections calculated in the frame of the generalized Mie theory for hybrid two-sphere dimers Pt-Ag (diameters  $\phi=80$  nm) for various interparticle distances ( $d=100$  nm (blue),  $d=4$  nm (green),  $d=2$  nm (magenta),  $d=1$  nm (cyan),  $d=0.5$  nm (red)). The incident electromagnetic field is polarized along the dimer axis and the optical index of the surrounding medium is  $n_{\text{ext}}=1.15$ . The optical extinction cross-section of the single platinum sphere (gray dotted line), silver sphere (black dotted line) and their sum (short dots) are also displayed.

## Conclusion

To conclude, we have shown that LSPRs can emerge in most transition metal-based NAs. Accurate calculations performed on spherical dimers (in the frame of the generalized Mie theory) have first demonstrated that we can take advantage of the plasmonic coupling to enhance LSPRs over a broad spectral range, for many transition metals (Pt, Pd, Cr, Ni, Co, Fe, ...). A comparative analysis of the optical response in gold and platinum spherical dimers shows that in both cases, the most

important effects in the optical response are the redshift and enhancement of the LSPR for decreasing interparticle distances. For gold, as the resonance arises below the interband transition threshold, its width is mainly correlated to radiative damping, and the well-defined hybridized modes can be identified in extinction spectra. In the case of transition metals such as platinum, the LSPR remains broad for low interparticle distances and the hybridized modes are now blurred in the overall resonance. However, an analysis of the charge distribution on the surface of the NPs shows that different hybridized modes constitute the whole LSPR band, even if their spectral contribution cannot be directly identified in extinction spectra since they are convoluted in the broad resonance. In the case of spherical dimers, the transfer of the oscillator strengths from the “dipolar” mode to higher orders involves a maximum extinction cross-section for intermediate interparticle distances of a few nanometers.

This plasmonic coupling has been then experimentally illustrated for three metals (Pt, Pd and Cr) on individual NAs of parallelepipedal geometry elaborated by nanolithography. Absolute extinction cross-sections have been measured over a broad spectral range (300-900 nm) on individual NAs the morphology of which has been independently characterized by electron microscopy imaging. First, as observed in the literature

## Acknowledgements

We would like to thank Armel Descamps-Mandine from the INL for AFM observations, Xavier Jaurand from the Technological Center of Microstructures (CT $\mu$ ) for technical assistance in SEM observations.

This work was supported by the LABEX iMUST (ANR-10-LABX-0064) of the university of Lyon, within the program "Investissements d'Avenir" (ANR-11-IDEX-0007) operated by the French National Research Agency (ANR). This work was also supported by the Lyon Centre NanOpTec and Nanolyon Centre facilities.

## Notes and references

<sup>a</sup> Université de Lyon, Université Lyon 1, Institut Lumière Matière (ILM), CNRS, UMR 5306, Bât A. Kastler, 43, bd du 11 Novembre 1918, 69622 Villeurbanne cedex, France.

<sup>b</sup> Université de Lyon, Université Lyon 1, Institut des Nanotechnologies de Lyon (INL), UMR 5270, CNRS-ECL-INSA-UCBL, 36 Av. Guy de Gollongue, Ecully; 69134, France.

<sup>\*</sup>Email of the corresponding author: [emmanuel.cottancin@univ-lyon1.fr](mailto:emmanuel.cottancin@univ-lyon1.fr)

Electronic Supplementary Information (ESI) available: [Additional figures: SEM images, FEM simulations, measured extinction cross-sections].

See DOI: 10.1039/b000000x/

1. E. Cottancin, M. Broyer, J. Lermé and M. Pellarin, in *Handbook of Nanophysics*, ed. K. D. Sattler, Taylor & Francis CRC Press, 2010, vol. Nanoelectronics and Nanophotonics, p. 24.
2. U. Kreibig and M. Vollmer, *Optical properties of Metal Clusters*, Springer, Berlin, 1995.
3. N. J. Halas, S. Lal, W. S. Chang, S. Link and P. Nordlander, *Chemical Reviews*, 2011, 111, 3913-3961.
4. I. Romero, J. Aizpurua, G. W. Bryant and F. J. G. d. Abajo, *Opt. Express*, 2006, 14, 9988-9999.
5. M. Ringle, A. Schwemer, M. Wunderlich, A. Nichtl, K. Kürzinger, T. A. Klar and J. Feldmann, *Phys. Rev. Lett.*, 2008, 100, 203002.
6. S. Acimovic, M. P. Kreuzer, M. U. Gonzalez and R. Quidant, *ACS Nano*, 2009, 3, 1231-1237.
7. S. Nie and S. R. Emory, *Science*, 1997, 275, 1102-1106.
8. A. M. Michaels, M. Nirmal and L. E. Brus, 1999, 121, 9932.
9. R. Elghanian, J. J. Storhoff, R. C. Mucic, R. L. Letsinger and C. A. Mirkin, *Science*, 1997, 277.
10. P. K. Jain and M. A. El-Sayed, *Nano Letters*, 2008, 8, 4347-4352.
11. M. E. Stewart, C. R. Anderton, L. B. Thompson, J. Maria, S. K. Gray, J. A. Rogers and R. G. Nuzzo, *Chem. Rev.*, 2008, 108, 494-521.
12. C. Sönnichsen, T. Franzl, T. Wilk, G. v. Plessen, J. Feldmann, O. Wilson and P. Mulvaney, *Physical Review Letters*, 2002, 88, 077402.
13. C. Sönnichsen and A. P. Alivisatos, *Nano Letters*, 2004, 5, 301-304.
14. O. L. Muskens, G. Bachelier, N. Del Fatti, F. Vallée, A. Brioude, X. Jiang and M.-P. Piliéni, *Journal of Physical Chemistry C*, 2008, 112, 8917.
15. A. M. Funston, C. Novo, T. J. Davis and P. Mulvaney, *Nano Letters*, 2009, 9, 1651-1658.
16. H. Tamaru, H. Kuwata, H. Miyazaki and K. Miyano, *Applied Physics Letters*, 2002, 80, 1826-1828.
17. T. Atay, J.-H. Song and A. V. Nurmikko, *Nanoletters*, 2004, 4, 1627-1631.
18. P. Nordlander, C. Oubre, E. Prodan, K. Li and M. I. Stockman, *Nanoletters*, 2004, 4, 899-903.
19. L. Gunnarsson, T. Rindzevicius, J. Prikulis, B. Kasemo, M. Käll, S. Zou and G. C. Schatz, *Journal of Physical Chemistry B*, 2005, 109, 1079.
20. P. K. Jain, W. Huang and M. A. E. Sayed, *Nanoletters*, 2007, 7, 2080.
21. C. Tabor, R. Murali, M. Mahmoud and M. A. El-Sayed, *J Phys Chem A*, 2009, 113, 1946-1953.
22. L. Yang, B. Yan and B. r. M. Reinhard, *The Journal of Physical Chemistry C*, 2008, 112, 15989-15996.
23. D. S. Kim, J. Heo, S. H. Ahn, S. W. Han, W. S. Yun and Z. H. Kim, *Nano Letters*, 2009, 9, 3619-3625.
24. E. R. Encina and E. A. Coronado, *The Journal of Physical Chemistry C*, 2010, 114, 3918-3923.
25. N. Grillet, D. Manchon, F. Bertorelle, C. Bonnet, M. Broyer, E. Cottancin, J. Lermé, M. Hillenkamp and M. Pellarin, *ACS Nano*, 2011, 5, 9450-9462.

26. K. Awazu, M. Fujimaki, C. Rockstuhl, J. Tominaga, H. Murakami, Y. Ohki, N. Yoshida and T. Watanabe, *Journal of the American Chemical Society*, 2008, 130, 1676-1680.
27. S. Baldelli, A. S. Eppler, E. Anderson, Y. R. Shen and G. A. Somorjai, *Journal of Chemical Physics*, 2000, 113, 5432-5438.
28. N. Liu, M. L. Tang, M. Hentschel, H. Giessen and A. P. Alivisatos, *Nature Materials*, 2011, 10, 631-636.
29. A. Alu and N. Engheta, *Optics Express*, 2009, 17, 5723-5730.
30. V. V. Temnov, G. Armelles, U. Woggon, D. Guzatov, A. Cebollada, A. Garcia-Martin, J.-M. Garcia-Martin, T. Thomay, A. Leitenstorfer and R. Bratschitsch, *Nature Photonics*, 2010, 4, 107-111.
31. N. C. Bigall, T. Hartling, M. Klose, P. Simon, L. M. Eng and A. Eychmuller, *Nano Letters*, 2008, 8, 4588-4592.
32. C. Langhammer, B. Kasemo and I. Zoric, *Journal of Chemical Physics*, 2007, 126.
33. C. Langhammer, Z. Yuan, I. Zoric and B. Kasemo, *Nano Letters*, 2006, 6, 833-838.
34. Y. Xiong, J. Chen, B. Wiley, Y. Xia, Y. Yin and Z.-Y. Li, *Nano Letters*, 2005, 5, 1237-1242.
35. I. Zoric, E. M. Larsson, B. Kasemo and C. Langhammer, *Advanced Materials*, 2010, 22, 4628-4633.
36. I. Zoric, M. Zäch, B. Kasemo and C. Langhammer, *ACS Nano*, 2011, 5, 2535-2546.
37. S. Jung, K. L. Shuford and S. Park, *J. Phys. Chem. C*, 2011, 115, 19049-19053.
38. P. Billaud, S. Marhaba, N. Grillet, E. Cottancin, C. Bonnet, J. Lermé, J.-L. Vialle, M. Broyer and M. Pellarin, *Review of Scientific Instruments*, 2010, 81, 043101.
39. P. Billaud, S. Marhaba, E. Cottancin, L. Arnaud, G. Bachelier, C. Bonnet, N. Del Fatti, J. Lermé, F. Vallée, J.-L. Vialle, M. Broyer and M. Pellarin, *J. Phys. Chem. C*, 2008, 112, 978-982.
40. P. Romaniello, P. L. de Boeij, F. Carbone and D. van der Marel, *Physical Review B*, 2006, 73, 075115-075111-075115-075116.
41. L. Hodges, R. E. Watson and Ehrenrei.H, *Physical Review B*, 1972, 5, 3953-&.
42. J. E. Nestell and R. W. Christy, *Physical Review B*, 1980, 21, 3173-3179.
43. J. H. Weaver, *Physical Review B*, 1975, 11, 1416-1425.
44. C. F. Bohren and D. P. Huffman, *Absorption and scattering of light by small particles*, Wiley, New York, 1983.
45. C. M. software.
46. P. B. Johnson and R. W. Christy, *Phys. Rev. B*, 1972, 6, 4370-4379.
47. P. B. Johnson and R. W. Christy, *Physical Review B*, 1974, 9, 5056-5070.
48. E. D. Palik, *Handbook of optical constants of solids*, Academic Press, New York, 1985-1991.
49. M. Meier and A. Wokaun, *Optics Letters*, 1983, 8, 581-583.
50. R. L. Chern, X. X. Liu and C. C. Chang, *Phys. Rev. E*, 2007, 76, 016609.
51. J. M. Gerardy and M. Ausloos, *Phys. Rev. B*, 1981, 25, 4204-4229.
52. S. Marhaba, G. Bachelier, C. Bonnet, M. Broyer, E. Cottancin, N. Grillet, J. Lermé, J.-L. Vialle and M. Pellarin, *Journal of Physical Chemistry C*, 2009, 113, 4349-4356.
53. Y. L. Xu, *Applied Optics*, 1997, 36, 9496-9508.
54. E. Prodan and P. Nordlander, *The Journal of Chemical Physics*, 2004, 120, 5444-5454.
55. J. A. Scholl, A. Garcia-Etxarri, A. L. Koh and J. A. Dionne, *Nano Letters*, 2013, 13, 564-569.
56. S. Kessentini, D. Barchiesi, C. D'Andrea, A. Toma, N. Guillot, E. Di Fabrizio, B. Fazio, O. M. Marago, P. G. Gucciardi and M. L. de la Chapelle, *Journal of Physical Chemistry C*, 2014, 118, 3209-3219.
57. T. Saito, S. Takahashi, T. Obara, N. Itabashi and K. Imai, *Nanotechnology*, 2011, 22, 445708.
58. G. Bachelier, I. Russier-Antoine, E. Benichou, C. Jonin, N. D. Fatti, F. Vallée and P.-F. Brevet, *Phys. Rev. Lett.*, 2008, 101, 197401.
59. L. V. Brown, H. Sobhani, J. B. Lassiter, P. Nordlander and N. J. Halas, *Acs Nano*, 2010, 4, 819-832.
60. B. Luk'yanchuk, N. I. Zheludev, S. A. Maier, N. J. Halas, P. Nordlander, H. Giessen and C. T. Chong, *Nature Materials*, 2010, 9, 707-715.
61. T. Shegai, P. Johansson, C. Langhammer and M. Käll, *Nano Letters*, 2012, 12, 2464-2469.